ArticleCode : pqa_3984

Firefly Algorithm-Based Voltage and Frequency Control of a Hybrid AC-DC Microgrid

M. Akbari, M.A. Golkar, and S.M. Moghaddas Tafreshi
Electrical and Computer Engineering Department
K.N. Toosi University of Technology
Tehran, Iran
mohsenakbari@ieee.org

***Abstract*—In this paper, an islanded microgrid with the hybrid AC and DC buses is studied. The voltage and frequency control of the AC or/and DC bus are one of the most important issues in all microgrids. Therefore, control schemes, used in this study, are developed in order to improve the voltage and frequncy stability of the proposed microgrid. Furthermore, a firefly optimization algorithm (FOA) solution is proposed to optimize the various controller parameters. The achieved results verify the controllers' robustness and optimization algorithm efficiency under the uncertainties existed in microgrid.**

***Index Terms*—controller, firefly algorithm, frequency control, microgrid, voltage control**

I. Introduction

For the past few years, due to serious traditional energy shortage and the stability problem existing in the utility grid, distributed generation is developed immediately. However, it also brings problems such as low stability and low power quality to the utility grid. Afterwards, with the achievements of distributed generation and the developing trend of modern power system, microgrid- a new conceptual solution, which is one type of future power systems put forward by researchers and inherits the advantages of distributed generation, has earning more and more attention. It has a special superiority on not only improving power quality and reliability but also relieving the pressure of energy and environment [1].

A microgrid is defined as two or more distributed generations or storage assets configured in a network and capable of operating either in parallel with, or independent from, a larger electric grid, while providing continuous power to one or more end users [2].

Multiple reverse conversions required in individual AC or DC grids may add additional loss to the system operation and will make the current home and office appliances more complicated [8].

In [3] a hybrid AC/DC microgrid is proposed to reduce processes of multiple reverse conversions in an individual AC or DC microgrid and to facilitate the connection of various renewable AC and DC sources and loads to power systems. Also, since in all the microgrids, the voltage and frequency control are one of the most important issues, so in this study, the voltage and frequency control of a hybrid microgrid is studied.

Beside, nature-inspired metaheuristic algorithms are becoming powerful in solving modern global optimization problems [4-5]. The firefly optimization algorithm (FOA) is a nature-inspired metaheuristic algorithm, inspired by the flashing behaviour of fireflies. The primary purpose for a firefly's flash is to act as a signal system to attract other fireflies. X.-S. Yang formulated this algorithm by assuming [6]:

1. All fireflies are unisexual, so that one firefly will be attracted to all other fireflies;
2. Attractiveness is proportional to their brightness, and for any two fireflies, the less brighter one will be attracted by (and thus move to) the brighter one; however, the brightness can decrease as their distance increases;
3. If there are no fireflies brighter than a given firefly, it will move randomly.

II. Microgrid Configuration

A hybrid microgrid as shown in Fig. 1 is proposed and modeled in MATLAB/Simulink. A 35 kW PV array is connected to DC bus through a DC/DC boost converter to simulate DC sources.

Also, a 45 kW wind turbine (WT) with DFIG is connected to an AC bus to simulate AC sources. In addition, a battery and a super-capacitor (SC) as the energy storages are separately connected to DC bus through bidirectional (buck-boost) DC/DC converters. DC and AC loads are also connected to DC and AC buses, respectively. The DC load was considered as a pure resistive load, but the connected AC load was included constant-impedance (resistance-inductance), constant-capacitance, and constant-power (induction motor) loads. The rated voltages for DC and AC parts are 400 V and 400 V rms, respectively. A 3-phase bidirectional DC/AC main converter with R-L-C filter connects the DC part to the AC part through an isolation transformer.

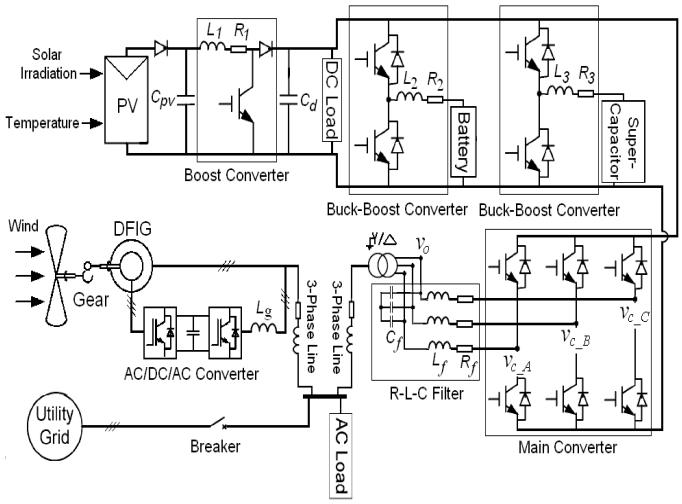

Fig. 1. A compact representation of the proposed hybrid microgrid

Fig. 2 shows an equivalent circuit of a PV array modeled by a controlled current source. i_{pv} and v_{pv} are terminal current and voltage of the PV array, respectively. The current output of the PV array was modeled by [7]:

$$I_{pv} = n_p I_{ph} - n_p I_{sat}\left[\exp\left(\left(\frac{q}{AkT}\right)\left(\frac{V_{pv}}{n_s} + I_{pv}R_s\right)\right) - 1\right] \quad (1)$$

$$I_{ph} = \left(I_{sso} + k_i\left(T - T_r\right)\right)\cdot\frac{S}{1000}$$

$$(2)\lambda_{qr} = \mathrm{L_r I_{qr}} + \mathrm{L_m I_{qs}}$$

$$I_{sat} = I_{rr}\left(\frac{T}{T_r}\right)^3 \exp\left(\left(\frac{qE_{gap}}{kA}\right)\cdot\left(\frac{1}{T_r} - \frac{1}{T}\right)\right)$$

$$(3)\lambda_{qr} = \mathrm{L_r I_{qr}} + \mathrm{L_m I_{qs}}$$

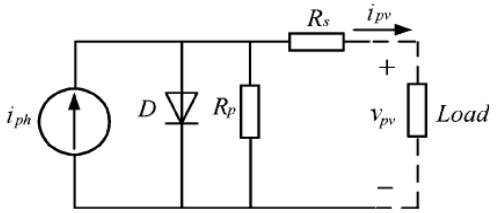

Fig. 2. Equivalent circuit of a PV array

Although renewable resources are attractive, they are not always dependable in the absence of energy storage devices. The utilization of energy storage units in power systems can be classified into two categories. One is in response to fast transients and the other is related to steady-state energy exchange. SCs are good candidates for the former application and batteries are suitable for the latter one. Currently, the mixed use of fast and slow energy storage units is gaining popularity for interconnection of renewable generation [8].

In this study, a 50 Ah, 200 V nickel-metal-hydride (NiMH) battery was used together with an SC storage. The battery was modeled using a controlled nonlinear voltage source in series with a constant resistance as shown in [9].

Also, in modeling of the present 7 F, 200 V SC storage, it was assumed that it is an ideal capacitance, i.e. its resistance was exactly considered to zero.

In this study, DFIG was considered as a wound rotor induction machine, which needs to excite at both the stator and rotor terminals. The modeling of DFIG is well shown in [9].

III. CONTROLLERS

The hybrid microgrid can operate in two modes: grid-connected mode and islanded mode. However, the islanding mode is studied in this paper. When the microgrid works in islanded operation mode, DC part voltage is regulated by the energy storages located in the DC part, while the AC bus voltage is controlled by the parallel inverter (main converter). The controllers used are described in the following sub-sections.

A. Boost Converter Controller

In this study, the control objective of the boost converter was assumed to track the maximum power point (MPPT) of the PV array. To achieve this objective, P&O method proposed in [10]-[11] was used, as shown in Fig. 3.

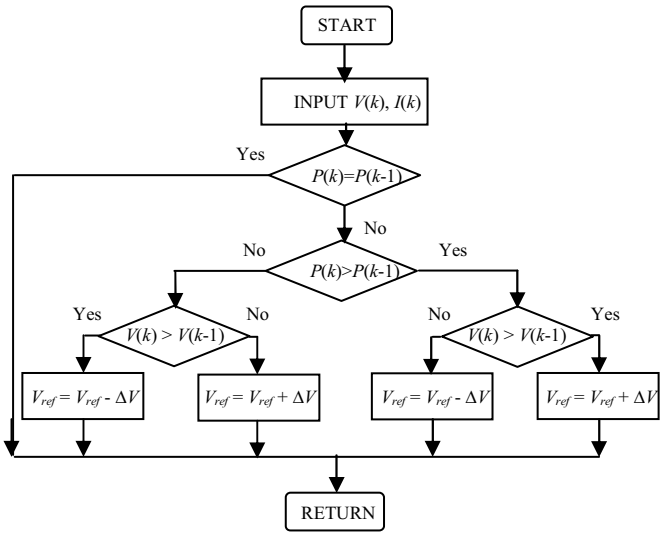

Fig. 3. MPPT Algorithm for the PV array

B. Coordinated Control of Battery and SC Storages

Battery has high energy density, whereas it has relatively slow charging and discharging speed. On the other hand, SC has high power density and fast response. The mixed use of these energy storage units can make them complimentary to each other. Based on the above characteristics of battery and SC, a hybrid control scheme was designed as shown in Fig. 4.

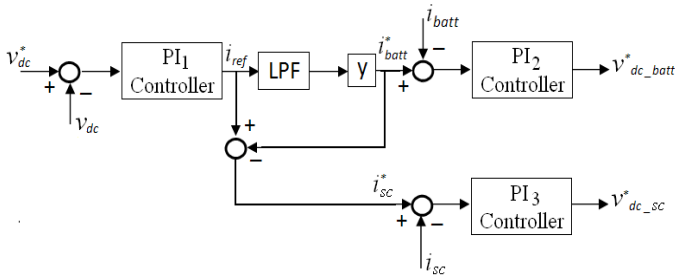

Fig. 4. Coordinated control scheme of the battery and SC storages

In this scheme, the DC part voltage is coordinately controlled by battery and SC storages. First, the measured DC part voltage v_{dc} is compared with its reference v^*_{dc} and the difference is sent to a proportional-integration (PI) controller to get the current reference i_{ref}. Then i_{ref} is split into two parts. One is the battery current reference i^*_{batt} which is obtained by applying a low-pass filter (LPF) with a cut-off frequency 25 Hz and a coefficient y (equal to 0.97 in this study) to i_{ref}. The other one i^*_{sc} is the difference between i_{ref} and i^*_{batt}. By this means, the high frequency part of the DC part disturbance and somehow low frequency part will be mitigated by the SC storage and the remained low frequency part of the disturbance is smoothed by battery. The current references i^*_{sc} and i^*_{batt} will be used in the constant current control of the buck-boost converters shown in Fig. 1.

C. Main Converter

Multi-loop voltage control for a DC/AC inverter is described in [12], where the control objective is to provide a high quality AC voltage with good dynamic response at different load conditions. This control scheme was also applied for the main converter to provide high quality AC voltage in islanded mode, as shown in Fig. 5.

D. DFIG Controller

DFIG has several controllers that are: rotor-side converter controller, grid-side converter controller, pitch controller and torque controller. The objectives of the rotor-side converter are to manage the stator-side active and reactive powers. The DTC scheme proposed in [7] was selected as the control method for the rotor-side converter in this study, as shown in Fig. 6. The rotor rotational speed, ω_r, was obtained through the MPPT algorithm, based on algorithm proposed in [13], to track the MPPT of WT. ω_r and the mechanical power P_m are used to calculate the electromagnetic torque T^*_{em}. The rotor side reference d-axis current ($i_{dr}^{*\varphi}$) is determined by T^*_{em} and the estimated stator flux linkage (λ_s). In Fig. 8, φ shows the variables in stator voltage oriented reference frame. Also, it is important to say that the reference reactive power Q^*_s was considered to 0.06.

The grid-side converter was designed to regulate the voltage of its own DC-link capacitor. In addition, this model allows using grid-side converter to generate or absorb reactive power. This control system is illustrated in Fig. 7. The voltage of the DC-link is controlled by i_{dg}, while the reactive power is controlled by i_{qg}.

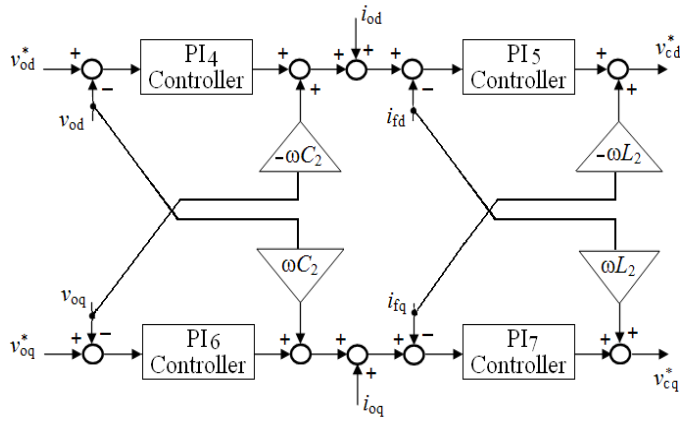

Fig. 5. Control scheme of main converter in islanded mode

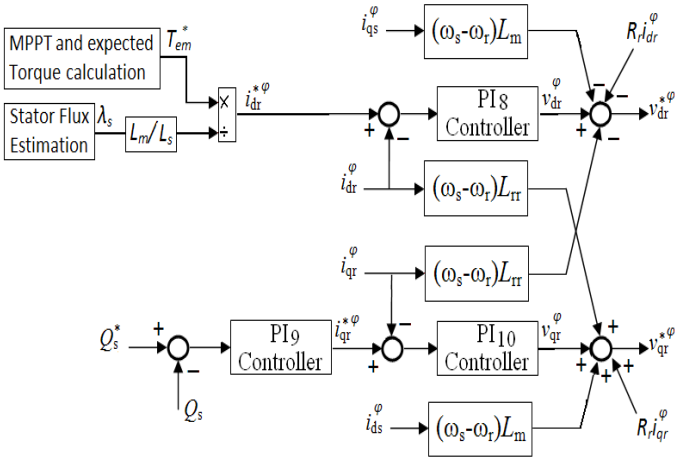

Fig. 6. The DTC control scheme for the rotor side converter

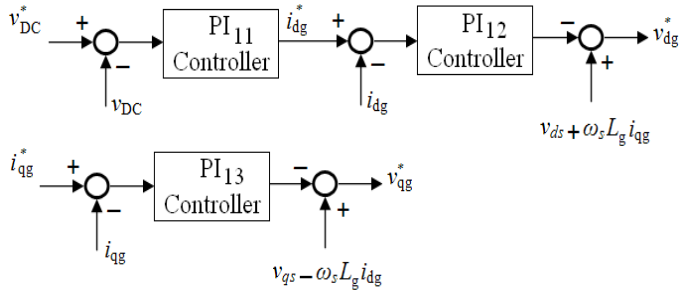

Fig. 7. Grid-side converter control block diagram

Also, pitch control scheme proposed in [14] was used for DFIG. The controller enforces the rotor speed related to MPPT as a reference speed. Also, pitch compensation was done in this scheme. When the available wind power is less than rated, the blades are fixed to maximize the mechanical power, and when the available wind power is above the equipment rating, the blades are pitched to reduce P_{mech} delivered to the shaft down to the mechanical power 1.0 pu.

Furthermore, the torque control scheme proposed in [14] was accomplished by using rotor speed reference. The torque controller output was used in rotor-side converter controller to calculate the d-axis current reference.

IV. FIREFLY ALGORITHM

The flashing light of fireflies is an amazing sight in the summer sky in the tropical and temperate regions. There are about two thousand firefly species, and most fireflies produce short and rhythmic flashes. The pattern of flashes is often unique for a particular species. The flashing light is produced by a process of bioluminescence, and the true functions of such signaling systems are still debating. However, two fundamental functions of such flashes are to attract mating partners (communication), and to attract potential prey. In addition, flashing may also serve as a protective warning mechanism. The rhythmic flash, the rate of flashing and the amount of time form part of the signal system that brings both sexes together. Females respond to a male's unique pattern of flashing in the same species, while in some species such as photuris, female fireflies can mimic the mating flashing pattern of other species so as to lure and eat the male fireflies who may mistake the flashes as a potential suitable mate.

The flashing light can be formulated in such a way that it is associated with the objective function to be optimized, which makes it possible to formulate new optimization algorithms.

Now we can idealize some of the flashing characteristics of fireflies so as to develop firefly-inspired algorithms. For simplicity in describing our FOA, we now use the following three idealized rules [6]: 1) all fireflies are unisex so that one firefly will be attracted to other fireflies regardless of their sex; 2) attractiveness is proportional to their brightness, thus for any two flashing fireflies, the less brighter one will move towards the brighter one. The attractiveness is proportional to the brightness and they both decrease as their distance increases. If there is no brighter one than a particular firefly, it will move randomly; 3) the brightness of a firefly is affected or determined by the landscape of the objective function. For a maximization problem, the brightness can simply be proportional to the value of the objective function. Other forms of brightness can be defined in a similar way to the fitness function in genetic algorithms or the bacterial foraging optimization algorithm (BFOA) [15].

In the FOA, there are two important issues: the variation of light intensity and formulation of the attractiveness. For simplicity, we can always assume that the attractiveness of a firefly is determined by its brightness which in turn is associated with the encoded objective function.

In the simplest case for maximum optimization problems, the brightness I of a firefly at a particular location x can be chosen as $I(x) \propto f(x)$. However, the attractiveness β is relative; it should be seen in the eyes of the beholder or judged by the other fireflies. Thus, it will vary with the distance r_{ij} between firefly i and firefly j. In addition, light intensity decreases with the distance from its source, and light is also absorbed in the media, so we should allow the attractiveness to vary with the degree of absorption. In the simplest form, the light intensity $I(r)$ varies according to the inverse square law $I(r) = I_s/r^2$.

where I_s is the intensity at the source. For a given medium with a fixed light absorption coefficient γ, the light intensity I varies with the distance r. That is [8]:

$$I = I_0 e^{-\gamma r} \tag{4}$$

where I_0 is the original light intensity.

As a firefly's attractiveness is proportional to the light intensity seen by adjacent fireflies, we can now define the attractiveness β of a firefly by [8]:

$$\beta = \beta_0 e^{-\gamma r^2} \tag{5}$$

where β_0 is the attractiveness at $r = 0$.

The pseudo code of the firefly algorithm can be summarized as shown in Fig. 8.

```
Begin
1) Objective function: f(x),  x = (x_1, x_2, ..., x_d);
2) Generate an initial population of fireflies x_i  (i = 1, 2, ..., n);.
3) Formulate light intensity I so that it is associated with f(x)
  (for example, for maximization problems, I ∝ f(x) or simply
I = f(x);
4) Define absorption coefficient γ
While (t<MaxGeneration)
  for i=1:n (all n fireflies)
    for j=1:n (n fireflies)
      if (I_j > I_i),
       move firefly i towards j;
      end if
    Vary attractiveness with distance r via exp(-γr);
    Evaluate new solutions and update light intensity;
    end for j
  end for i
  Rank fireflies and find the current best;
end while
Post-processing the results and visualization;
end
```

Fig. 8. FOA pseudo code

The main update formula for any pair of two fireflies x_i and x_j is [8]:

$$x_i^{t+1} = x_i^t + \beta \exp\left[-\gamma r_{ij}^2\right] + \alpha_t \varepsilon_t \tag{6}$$

where α_t is a parameter controlling the step size, while ε_t is a vector drawn from a Gaussian or other distribution.

It can be shown that the limiting case $\gamma \to 0$ corresponds to the standard particle swarm optimization (PSO). In fact, if the inner loop (for j) is removed and the brightness I_j is replaced by the current global best g^*, then FOA essentially becomes the standard PSO.

In this study, we took β_0=1, α_t=0.7, and γ=1. The parameter γ now characterizes the variation of the attractiveness, and its value is crucially important in determining the speed of the convergence and how the FOA algorithm behaves. The searching procedure for the FOA technique is summarized as follows:

Step1: Initialization: A population *N* of M-dimension firefly positions and velocities are randomly initialized having. In this study, *N* was set to be 40. M is the number of parameters which we want to optimize them. Since, the parameters of PI controller 1, 2, 3, 4, 5, 6 and 7 (totally 14 parameters) have the most effect on voltage and frequency control, these parameters were considered to optimize. It is important to say that the PI controller 5 and 7 have the same parameters, so totally 12 parameters were considered to optimize.

In the initialization, the upper and lower bounds, $x_{\max}$ and x_{min} respectively, of the parameters should be specified at first; these define the searching space. In this study, position of proportional and integral gains (k_p and k_i) were respectively limited in [0, 50] and [0, 900].

Step2: Evaluation: Our objective from the FOA algorithm was to find optimal parameters in order to restore and stabilize the voltage and frequency quickly. The islanding event was considered for the optimization process of the parameters: The optimization of the controllers can be done by minimizing an error-integrating cost function. Four common types of these functions are: integrated absolute error (IAE), integrated squared error (ISE), integrated time-weighted absolute error (ITAE), and integrated time-weighted squared error (ITSE) [16]. Since ITAE yields the best performance for the considered objectives, so it was selected to be minimized as error-integrating cost function in FOA algorithm. Also, since once the islanding is occurred, DC and AC parts voltage and AC part frequency will intensely change, so their improvement was considered in PSO algorithm. Since the frequency error has a less amplitude and is more important than the voltage error amplitude, therefore the frequency error was multiplied by 100 and the AC and DC voltages error was multiplied by 1. This fitness function was mathematically defined as follows:

$$error = error_{v\_dc} + error_{v\_ac} + error_{f\_ac} \tag{7}$$

$$error_{v\_dc} = \sum_t t * \left| v_{dc\_measured}(t) - v_{dc\_ref}(=400) \right| \tag{8}$$

$$error_{v\_ac} = \sum_t t * \left| v_{ac\_l\text{-}l\_measured}(t) - v_{ac\_ref}(=400) \right| \tag{9}$$

$$error_{f\_ac} = 100 * \sum_t t * \left| f_{ac\_measured}(t) - f_{ac\_ref}(=60) \right| \tag{10}$$

where, t is the simulation time with step-time set to $1.0*10^{-4}$ s. Also, $v_{dc\text{-}measured}$, $v_{AC\_measured}$, $f_{AC\_measured}$, v_{dc_ref}, v_{AC_ref}, f_{AC_ref} are the measured DC voltage, measured line-to-line AC voltage, measured AC frequency, reference DC voltage (400 V), reference line-to-line AC voltage (400 V), and reference AC frequency, respectively.

Step3: Stopping criterion: The stopping criterion was determined by $Iter_{max}$. If the iteration number is ended, then program will be stop, else go to Step 4.

Step 4: Update: The updating was done by (6) while the upper and lower limits were handled as follows:

$$\begin{aligned} &if \;\; x_{i,j}(t+1) > x_{j,\max} \;\; then \;\; x_{i,j}(t+1) = x_{j,\max} \\ &if \;\; x_{i,j}(t+1) < x_{j,\min} \;\; then \;\; x_{i,j}(t+1) = x_{j,\min} \end{aligned} \tag{11}$$

Then, go to Step 2.

V. Dynamic Simulations

In this section, simulations performed in MatLab/Simulink, are shown to verify the improvement in voltage and frequency stability. The optimized parameters of PI controllers are shown in appendix. At the first, the fluctuation of the solar irradiation level is considered. In second 6, the irradiation level is decreased from 800 kW/m2 to 200 kW/m2, and then increased to 800 kW/m2 in second 7. The DC voltage, battery current and SC current response to these disturbances are shown in Figs. 9-11. When the PV power generation and as a result the power supplied to DC load is suddenly decreased, the DC voltage is also decreased. The battery and SC storages will compensate this generation reduction by increasing their power generation as shown in Figs. 10-11. Furthermore, when the PV generation is increased, the above process is adversely done.

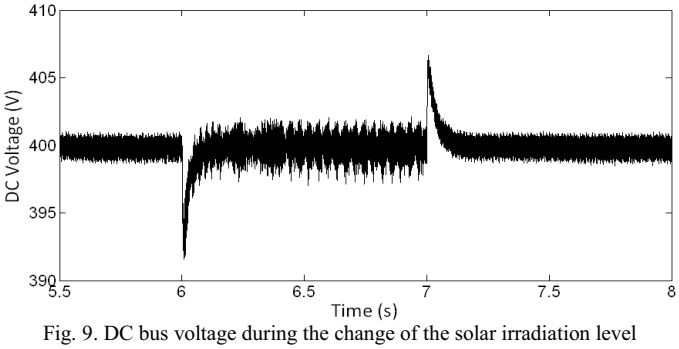

Fig. 9. DC bus voltage during the change of the solar irradiation level

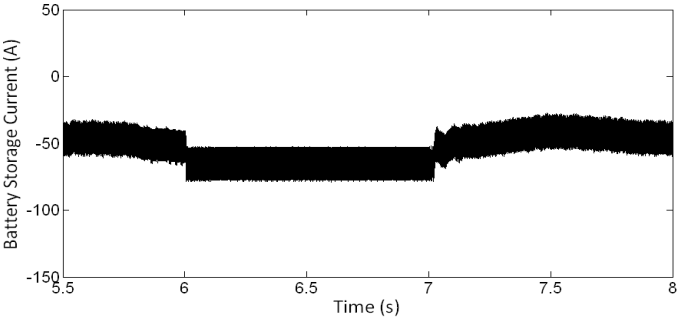

Fig. 10. Battery storage current during the change of the solar irradiation level

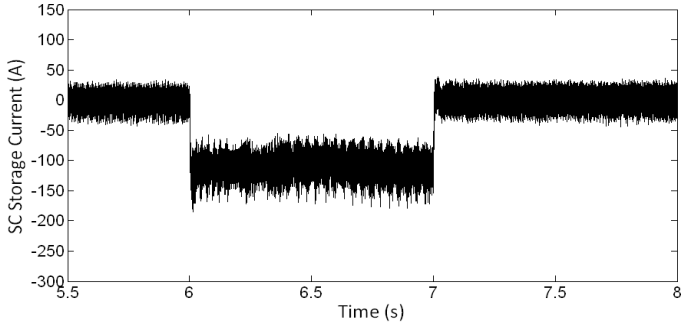

Fig. 11. SC storage current during the change of the solar irradiation level

Now, the DC load change is studied. In second 6, the DC load is increased from 10 kW to 20 kW and then decreased to 20 kW in second 7. The DC voltage, battery current and SC current response to these disturbances by the optimized-PI controllers are shown in Figs. 12-14. When the DC load is increased, the consumed power is more than the supplied power in DC part. Therefore, the DC voltage is decreased in second 6. But it is quickly compensated by SC and battery storages. Also, when the dc load is decreased to 10 kW in second 7, the above process is adversely done.

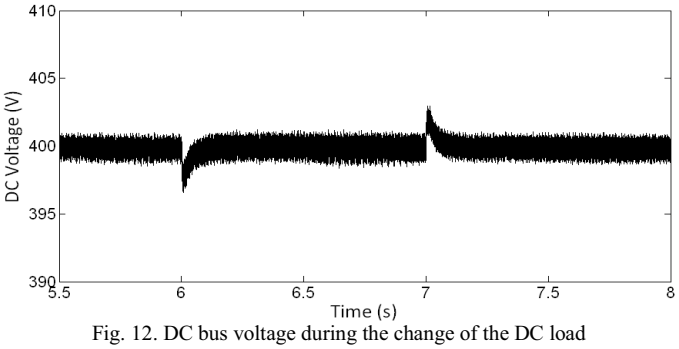

Fig. 12. DC bus voltage during the change of the DC load

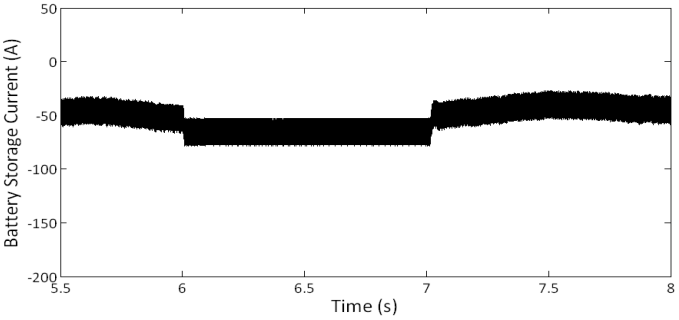

Fig. 13. Battery storage current during the change of the DC load

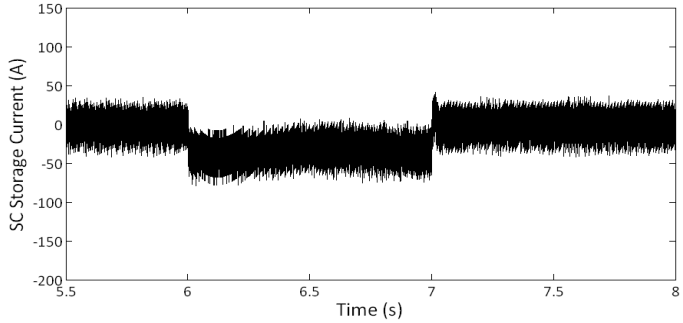

Fig. 14. SC storage current during the change of the DC load

Furthermore, the AC load change is studied. In second 6, the AC load is increased from 30 kW to 50 kW and then decreased to 30 kW in second 7. The AC voltage and AC frequency response to these disturbances by the optimized-PI controllers are shown in Figs. 15-16. When the AC load is increased, in a very short time the consumed power is more than the supplied power in AC part. Therefore, the AC voltage is decreased in second 6. But it is quickly compensated by SC and battery storages. Also, when the AC load is decreased to 20 kW in second 7, the above process is adversely done.

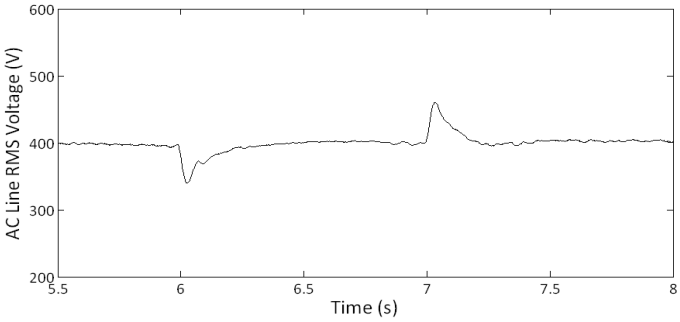

Fig. 15. AC bus voltage during the change of the AC load

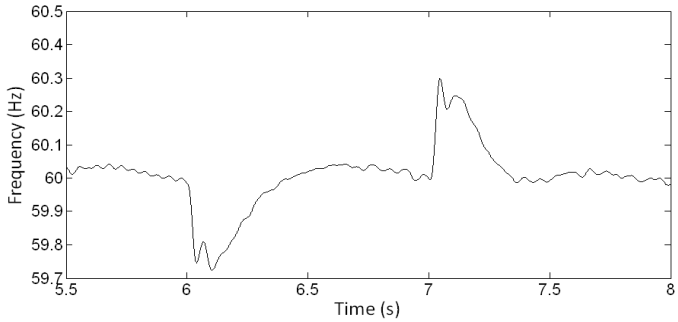

Fig. 16. AC bus frequency during the change of the AC load

Finally, the fault occurrence is studied. In second 6, a permanent 3-phase fault is occurred in AC part (between the main converter and the isolation transformer) and then cleared in second 6.15. The AC voltage, AC frequency and DC voltage response to this disturbance are shown in Figs. 17-19. The results show that the optimized-PI controllers have the high performance and robustness to the disturbances.

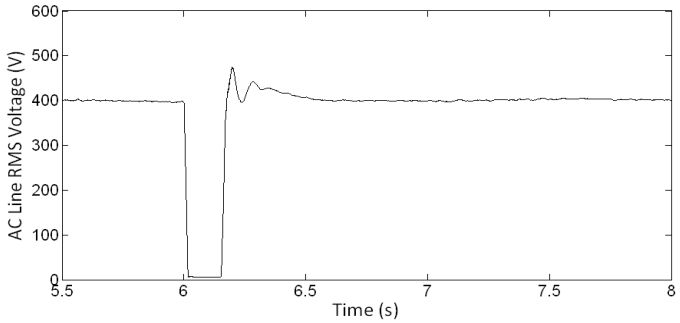

Fig. 17. AC bus voltage during the 3-phase fault occurrence

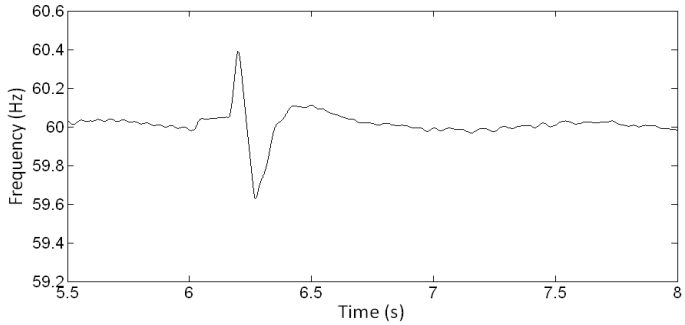

Fig. 18. AC bus frequency during the 3-phase fault occurrence

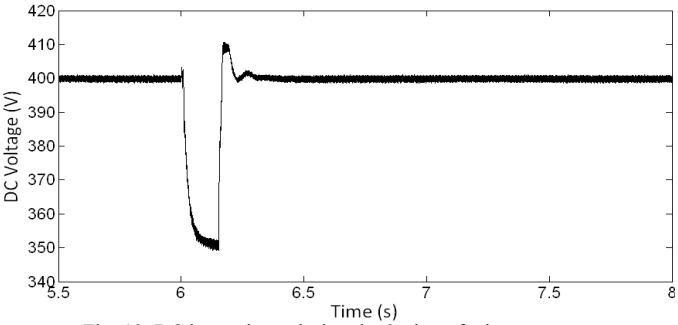

Fig. 19. DC bus voltage during the 3-phase fault occurrence

VI. CONCLUSION

In this paper, controllers of a hybrid AC/DC microgrid were designed to improve the voltage and frequency stability. Since the parameters of PI controllers play an important role in stability and control of the systems, so a FOA algorithm was selected to optimize them in order to quickly restore and stabilize the voltage of both AC and DC buses and AC bus frequency. The results achieved show the efficiency of optimized controllers compared to the controllers having the original parameters when the microgrid is subjected to the disturbances.

REFERENCES

[1] M. J. Yang, F. Zhuo, X. W. Wang, H. P. Guo, and Y. J. Zhou, "Research of seamless transfer control strategy of microgrid system," *in Proc. 2011 IEEE 8th Int. Conf. Power Electronics and ECCE Asia (ICPE & ECCE)*, pp. 2059-2066, 2011.

[2] Northern Power System Inc., Waltsfield, VT. http://www.northernpower.com/pdf/pr_Microgrid.pdf.

[3] M. Akbari, M. A. Golkar, and S. M. M. Tafreshi, "Voltage control of a hybrid ac/dc microgrid in grid-connected operation mode," in *Proc. 2011 IEEE PES Innovative Smart Grid Technologies - India (ISGT India)*, India, pp. 358-362, 2011.

[4] J. Kennedy, R. Eberhart, and Y. Shi, *Swarm Intelligence*, Morgan Kaufmann Academic Press, San Francisco, 2001.

[5] X.S. Yang, *Nature-Inspired Metaheuristic Algorithms*, Luniver Press, Beckington, UK, 2008.

[6] Yang, X. S. (2008). *Nature-Inspired Metaheuristic Algorithms*. Frome: Luniver Press.

[7] X. Liu, P. Wang, and P. C. Loh, "A hybrid AC/DC microgrid and its coordination control," *IEEE Trans. Smart Grid*, vol. 2, no. 2, pp. 278-286, Jun. 2011.

[8] F. S. Garcia, A. A. Ferreira, and J. A. Pomilio, "Control strategy for battery-ultracapacitor hybrid energy storage system," in *Proc. 24th Annu. IEEE Appl. Power Electron. Conf. and Exposition (APEC)*, pp. 826-832, 2009.

[9] www.mathworks.com

[10] L. N. Khanh, J.-J. Seo, Y.-S. Kim, and D.-J. Won, "Power management strategies for a grid-connected PV-FC hybrid system," *IEEE Trans. Power Del.*, vol. 25, no. 3, pp. 1874-1882, July 2010.

[11] R. Majumder, F. Shahnia, A. Ghosh, G. Ledwich, M. Wishart, and F. Zare, "Operation and control of a microgrid containing inertial and non-inertial micro sources," in *Proc. IEEE Region 10 Conf. (TENCON)*, pp. 1-6, 2009.

[12] N. Pogaku, M. Prodanovic, and T. C. Green, "Modeling, analysis and testing of autonomous operation of an inverter-based microgrid," *IEEE Trans. Power Electron.*, vol. 22, no. 2, pp. 613-625, Mar. 2007.

[13] R. Carriveau, *Fundamental and Advanced Topics in Wind Power*, J. S. Thongam, and M. Ouhrouche, *MPPT Control Methods in Wind Energy Conversion Systems*, InTech, 2011.

[14] N. W. Miller, J. J. Sanchez-Gasca, W. W. Price, and R. W. Delmerico, "Dynamic modeling of GE 1.5 and 3.6 MW wind turbine generators for stability simulations," in *Proc. IEEE Power Eng. Soc. General Meeting*, pp. 1977-1983, vol. 3, 2003.

[15] K. Gazi, and K. M. Passino, "Stability analysis of social foraging swarms," *IEEE Trans. Syst., Man., Cybern. B, Cybern.,* vol. 34, no. 1, pp. 539-557, Feb. 2004.

[16] I.-Y. Chung, W. Liu, D. A. Cartes, and K. Schoder, "Control parameter optimization for a microgrid system using particle swarm optimization," in *Proc. IEEE Int. Conf. Sustainable Energy Technologies (ICSET)*, Singapore, pp. 837-842, 2008.

APPENDIX

The FOA-optimized parameters of the controllers:

k_{p1}=34.5, k_{i1}=111.16, k_{p2}=7.30, k_{i2}=66.00, k_{p3}=36.15, k_{i3}=443.38, k_{p4}=44.51,k_{i4}=254.00,k_{p5}=k_{p7}=1.83, k_{i5}=k_{i7}=875.71, k_{p6}=15.46, k_{i6}=824.19